Structural characterization of poly(ε-caprolactone)-grafted cellulose acetate and butyrate by solid-state ^{13}C NMR, dynamic mechanical, and dielectric relaxation analyses

Ryosuke Kusumi, Yoshikuni Teramoto, and Yoshiyuki Nishio*

Division of Forest and Biomaterials Science, Graduate School of Agriculture, Kyoto University, Kyoto 606-8502, Japan

**Author for correspondence (e-mail: ynishio@kais.kyoto-u.ac.jp; phone: +81-75-753-6250; fax: +81-75-753-6300)*

Abstract

Investigations were made into the molecular dynamics and intercomponent mixing state in solid films of two series of cellulosic graft copolymers, cellulose acetate-*g*-poly(*ε*-caprolactone) (CA-*g*-PCL) and cellulose butyrate-*g*-PCL (CB-*g*-PCL), both series being prepared over a wide range of compositions with CAs or CBs of acyl DS ≈ 2.1, 2.5, and 2.95. It was shown by $T_{1\rho}{}^{H}$ measurements in solid-state ^{13}C NMR spectroscopy that all the copolymer samples, except ones using CA of DS = 2.98, formed an amorphous monophase in which the trunk and graft components were mixed homogeneously at least in a scale of a few nanometers. However, those copolymer samples gave, more or less, a response of dynamic heterogeneity, when examined under mechanical oscillation. Through dielectric relaxation measurements, a clear comparison was made between the CA-*g*-PCL and CB-*g*-PCL series, regarding the cooperativeness in segmental motions of the trunk and graft chains, directly associated with the extent of the dynamic heterogeneity. The cooperativeness was generally higher in the CB-based copolymer series, probably due to working of the butyryl substituent as an internal compatibilizer.

Keywords

cellulose ester-*graft*-aliphatic polyester; molecular dynamics; heterogeneity

1. Introduction

Cellulose and its derivatives are environmentally benign substances and possess great potential to be developed for further industrial applications in conjugation with supplementary ingredients [1–3]. Polymer grafting of industrially well-established cellulose ester (CE) products, represented by cellulose acetate (CA), is a significant approach not only to improve the original physical properties including thermal processability of the cellulosics, but also to expand their availability as newly functionalized polymeric materials. The employment of aliphatic polyesters or poly(hydroxyalkanoate)s in a wide sense as the component for grafting onto CEs may be of particular importance, because the resulting copolymers can be a biodegradation-controllable material of great promise [4]. Usually, the graft density is changeable by varying the degree of substitution (DS) of the CE substrate used, the remaining hydroxyl groups serving as reactive sites for the graft copolymerization.

Recently, the authors' group has synthesized graft copolymers of CA and cellulose butyrate (CB) of acyl DS > 2 with poly(*ε*-caprolactone) (PCL), the products being termed CA-*g*-PCL and CB-*g*-PCL, respectively [5]; the two trunk CEs (CA and CB) are, respectively, immiscible and miscible with PCL in the corresponding binary polymer blends [5,6]. In that study [5] using copolymer compositions rich in PCL content, it was shown that all the products except copolymers based on CA of DS > 2.9 indicated an obviously single T_g in differential scanning calorimetry (DSC) measurements, but the melt-crystallization kinetics of the PCL component and resulting supramolecular morphology were largely different in the manner of the composition dependence between the two graft series. In a subsequent work [7], we investigated enzymatic hydrolysis behavior of PCL for melt-molded films of the above CE-*g*-PCLs by employing *Pseudomonas* lipase and demonstrated that the degradation rate and the surface morphology of the films were both subtly changeable by adequate selections of the compositional parameters and intercomponent miscibility of the original copolymer products.

Against the background stated above, the present paper focuses on the molecular dynamics and intercomponent mixing state in solid aggregates of the two CE-*g*-PCL series (prepared over a wider composition range), for further comprehension of the structural characteristics. The graft copolymers are composed of a semi-rigid cellulosic backbone and a very flexible aliphatic polymer as side chains. In such a combination, even though DSC analysis of the copolymers indicates a single T_g reflecting a considerably homogeneous

amorphous mixture, other dynamic measurements may detect separate responses from the two components due to the large difference in molecular mobility.

Formerly, several researchers have examined molecular relaxation behavior of CEs (mostly CA) by dynamic mechanical analysis (DMA) [8–10], dielectric relaxation spectroscopy (DRS) [11,12], and their combination [13], mainly in order to assign the structural origin of the relaxation processes. As for CE-based copolymers, a few attempts have been made to detect multiple relaxation signals for some CA samples grafted with PCL, by DMA [14–16]; however, little progress was made in the discussion of molecular dynamics correlated with the copolymer architecture, partly due to insufficient characterization of the chemical compositions used. As a matter of course, there was no reference to the dynamic heterogeneity for the CA-based copolymer solids.

In the present work, first, the mixing state of CE and PCL constituents in films of the CA-*g*-PCL and CB-*g*-PCL series are investigated by measurements of ^{1}H spin-lattice relaxation time in the rotating frame ($T_{1\rho}^{H}$) in solid-state ^{13}C NMR spectroscopy. Secondly, different relaxation processes are detected by DMA for film samples of both graft series and assigned to a motion referring to a relevant structural unit in the graft copolymers. DRS measurements are then conducted for the same samples over a wide frequency range (10^{-2}–10^{6} Hz), and the major relaxation processes observed are analyzed by using an approved model function. It should be noted here that there are differences not only in how to give perturbations but also in observation temperatures, between these three measurements. Namely, in the $T_{1\rho}^{H}$ analysis, a static homogeneity in the two copolymer series is observable through ^{1}H-spin diffusion at ambient temperature (20 °C). On the other hand, in the DMA and DRS measurements, the degree of dynamic heterogeneity is revealed via the observation of relaxation processes under mechanical and electric-field oscillations, respectively, over wide-ranging temperatures. Based on the experimental results, a comparison is made between the two CE-*g*-PCL series, regarding the dynamic heterogeneity in the mixture of the trunk and graft components and the extent of cooperativeness in their chain-segmental motions.

2. Experimental

2.1. CA-g-PCL and CB-g-PCL copolymers

The methods of synthesis and characterization of CA-*g*-PCLs and CB-*g*-PCLs have been

described in our previous study [5]. A starting material CA had an acetyl DS of 2.15, 2.45, and 2.98. CB samples of butyryl DS = 2.10, 2.50, and 2.93 were synthesized with acid chloride/base catalyst from cotton cellulose (M_v = 252000) via a homogeneous reaction. In both copolymer series, the degree of molar substitution (MS) for the introduced oxycaproyl units was varied between ~0.15 and ~9.0 per anhydroglucose unit. Table 1 summarizes data of the average molecular weights (M_w and M_n), and the copolymer composition parameters, i.e., acyl DS, oxycaproyl MS, the apparent degree of polymerization of the PCL side-chain (DP_s'), and the PCL content in weight percent (W_{PCL}), together with thermal data including glass transition and melting temperatures (T_g and T_m), for the copolymer and homopolymer samples used. A code CE_x-*g*-PCL_y denotes CE-*g*-PCL of acetyl or butyryl DS = *x* and oxycaproyl MS = *y*.

<< Table 1 >>

The basic thermal properties of the two CE-*g*-PCL series were characterized by DSC analysis in the same way as that described in the preceding paper [5]. In brief, any of the copolymer samples, except for $CA_{2.98}$-*g*-PCLs of MS > 2, showed a single T_g varying with oxycaproyl MS, indicating that no segregation behavior occurred at least in a scale distinguishable by T_g detection in DSC. The $CA_{2.98}$-*g*-PCLs of MS > 2 gave two independent T_gs and a small melting endotherm at ~260 °C; the products have quite a low graft-density and virtually behave like a block copolymer [5,17], giving rise to a phase separation of the CA and PCL components due to the inherent immiscibility [6]. With regard to the compositions of MS > 7 in both CE-*g*-PCL series, the PCL component was allowed to develop a crystalline phase when cooled from the respective molten bulks.

2.2. Preparation of film samples

Except for $CA_{2.98}$ and a few copolymer products based on the CA, the two CE-*g*-PCL series and plain PCL and CEs were thermally molded into a film form at 100–260 °C, i.e., above the T_g or T_m of each sample, by using a Toyo-Seiki hot-pressing apparatus with a stainless spacer 0.10 mm thick. For the molding, a pressure was applied to the respective molten samples gradually to reach 5.0 MPa in 3 min, and subsequently it was increased quickly to 15.0 MPa, followed by maintaining this application for 30 sec. Immediately after the pressure was released, the samples were transferred to another compressing apparatus and cold-pressed at 15.0 MPa and 25 °C for 10 min. The films thus molded were placed at 20 °C

in a drying desiccator for 48 h until used for the relaxation measurements described below.

Concerning $CA_{2.98}$, $CA_{2.98}$-*g*-$PCL_{0.22}$, and $CA_{2.98}$-*g*-$PCL_{0.55}$, it was difficult to mold them in the manner mentioned above, due to a certain extent of crystallinity as cellulose triacetate (see Table 1). Therefore, film samples of these three were prepared by solution casting with dichloromethane as solvent. Prior to the following measurements, however, the as-cast films (actually their strips) were heat treated at 300 °C *in vacuo* for 3 min to eliminate the triacetate crystal and placed under a dried condition at 20 °C for 48 h.

2.3. Measurements

High-resolution ^{13}C solid-state NMR measurements were carried out at ambient temperature (20 °C) with a JEOL JNM CMX-300 spectrometer operated at a frequency of 74.7 MHz. The magic angle spinning (MAS) rate was approximately 6 kHz. ^{13}C CP/MAS spectra were obtained in conditions of a contact time of 1.0 ms and a 90° pulse width of 5.0 μs. In quantification of proton spin-lattice relaxation times in the rotating frame, $T_{1\rho}^{H}$, a contact time of 0.1 ms was used and a proton spin-locking time (t) ranged from 1.0 to 30 ms for the copolymers and 1.0 to 100 ms for plain PCL. 1024 scans were accumulated for both CP/MAS spectra and $T_{1\rho}^{H}$ measurements.

DMA measurements were conducted by using a Seiko DMS6100/EXSTAR6000 apparatus. Rectangular film strips 20 × 4 mm^2 (ca. 100 μm thick) were used for measurements of the temperature dependence of the dynamic storage modulus (E') and loss modulus (E'') in the range −150–260 °C. The oscillatory frequency of the dynamic test was usually 10 Hz, and the temperature was raised at a rate of 2 °C·min^{-1}.

DRS measurements were made for film strips of square shape (10 × 10 mm^2) and ca. 100 μm thickness in a frequency range of 10^{-2}–10^{6} Hz, by using a Solartron 1255B Frequency Response Analyzer equipped with a Dielectric Interface (Solartron 1296). After putting the film sample in a measuring capacitor and inserting them into a LN-Z Cryostat with a LakeShore 331S Temperature Controller, the sample was quenched to –195 °C under a helium atmosphere. Then the complex permittivity (ε^*) was recorded every 2 °C in a stepwise heating process up to 200 °C.

3. Results and discussion

3.1. ^{13}C Solid-state NMR analysis

3.1.1. CP/MAS Spectra of CE-g-PCLs

Figure 1 illustrates ^{13}C CP/MAS spectra of $CA_{2.15}$-*g*-$PCL_{9.70}$ and $CB_{2.10}$-*g*-$PCL_{9.03}$, together with those of the original CA and CB materials and a PCL homopolymer. Peak assignments of the spectra were made based on literature data [6,18,19]. In the NMR spectra of the copolymer samples, a resonance peak of pyranose carbon C6 of the trunk CE components and that of methylene C6″ of the PCL component overlapped completely with each other to make a single peak at 65.3 ppm. In the spectrum of the CB-based copolymer, a resonance signal assigned to methylene C2′ in the butyryl group of the CB component was hidden behind a methylene C2″ signal (33.6 ppm) of the other component PCL, and, moreover, two carbonyl signals, C1′ of CB and C1″ of PCL, merged into a single peak at 173 ppm. However, resonance peaks of pyranose C2/C3/C5 (≈ 72.9 ppm) and acetyl C2′ (20.7 ppm) and butyryl C4′ (13.8 ppm) belonging to the respective CE trunks, and those of C3″/C4″ (≈ 25.8 ppm) and C5″ (≈ 29.1 ppm) in the PCL side-chain were all clearly detected for both copolymers. Thus the $T_{1\rho}{}^{H}$ measurements for the present CE-*g*-PCL series were carried out by monitoring these distinguishable five signals.

<< Figure 1 >>

3.1.2. Intercomponent mixing state as estimated by $T_{1\rho}{}^{H}$ measurements

The measurements of $T_{1\rho}{}^{H}$ for specific carbons in a multicomponent polymer system make it possible to estimate the mixing homogeneity in a scale of ^{1}H spin-diffusion length (= 2–4 nm). In general, $T_{1\rho}{}^{H}$ values can be obtained by fitting the decaying carbon resonance intensity to the following single-exponential equation:

$$M(t) = M(0)\exp(-t/T_{1\rho}{}^{H}) \quad (1)$$

where $M(t)$ is the magnetization intensity observed as a function of the spin-locking time t. The $T_{1\rho}{}^{H}$ is determined practically from the slope in the plot of $\ln[M(t)/M(0)]$ against t. In the present study, however, the logarithmic $M(t)$ data for PCL and some PCL-rich copolymers hardly fitted to a single straight-line, due to the presence of a distinct crystalline phase which should show a slower decay of magnetization. In such a case, the normalized $M(t)$ was simulated by a bi-exponential function involving two relaxation times, as follows [20]:

$$M(t)/M(0) = x_f \exp(-t/T_{1\rho}{}^{H}_{fast}) + x_s \exp(-t/T_{1\rho}{}^{H}_{slow}) \quad (2)$$

where $T_{1\rho}{}^{H}_{fast}$ and $T_{1\rho}{}^{H}_{slow}$ represent $T_{1\rho}{}^{H}$s of the flexible (faster decay) and rigid (slower

decay) components and x_f and x_s are the respective fractions.

Results of the $T_{1\rho}{}^{H}$ quantifications for CA-*g*-PCLs and CB-*g*-PCLs are compiled in Table 2. In both copolymer series, except for the compositions of MS > 7 in which crystallization of the PCL side-chains was inevitable in the melt-quenching and drying processes adopted, all the carbon resonance signals of the CE and PCL components provided only a single $T_{1\rho}{}^{H}$; the value decreased with an increase in MS, when compared between the samples with a common acyl DS = *x*. This decrease reflects that the molecular mobility of the CE_x-based graft copolymer was enhanced by the escalating introduction of the flexible PCL side-chains as internal plasticizer.

<< Table 2 >>

For the CA-*g*-PCLs of acetyl DS = 2.15 and 2.45 listed in Table 2, we can see no remarkable difference in value between the two sets of $T_{1\rho}{}^{H}$ data associated with the respective polymer components, as far as the composition range of MS < 3 is concerned. The microphase structure in these copolymer samples appears to be rather homogeneous, in a scale of the maximum path length *L* of the ^{1}H-spin diffusion; the length *L* is given by the equation [21]

$$L \cong (6\,D\,T_{1\rho}{}^{H})^{1/2} \qquad (3)$$

where *D* is the diffusion coefficient, usually taken to be ~10^{-12} cm^2/s in organic polymer materials. Simple application of the above equation, for example, with $T_{1\rho}{}^{H}$ values of ~2.7 ms (CA component) and ~2.0 ms (PCL component) for $CA_{2.15}$-*g*-$PCL_{2.50}$, leads to an estimation of $L \approx 1.3$ and 1.1 nm, respectively. Thus it is inferred from this NMR method that the copolymer sample shows only a little heterogeneity in a scale of a few nanometers. Obviously, the good homogeneity of such description is brought by virtue of the covalent linkage perpetuated compulsorily between the originally immiscible CA and PCL chains. However, this is not the case for $CA_{2.98}$-*g*-PCLs with an extremely low graft density; the virtually block-like copolymers showed a marked domain formability, as has been described in our previous study [5]. In Table 2, correspondingly, we find a definitely large discrepancy between the two sets of $T_{1\rho}{}^{H}$ data associated with the respective components, $CA_{2.98}$ trunk and PCL graft; e.g., an averaged value 13.2 ms (CA component) is much larger than 7.0 ms (PCL component), observed for $CA_{2.98}$-*g*-$PCL_{0.55}$.

Concerning the other copolymer series based on CB, $T_{1\rho}{}^{H}$ data evaluated for the two components were very close to each other, irrespective of the graft density (i.e., butyryl DS),

but in the composition range of MS < 4. For example, even for $CB_{2.93}$-*g*-$PCL_{3.58}$ with a low graft density, we obtained $T_{1\rho}{}^{H} \approx 3.0$ ms (CB component) and 3.3 ms (PCL component); this offers full assurance of a homogeneity within the spin-diffusion limits less than a few nanometers, reflecting the intrinsically better miscibility of the CB/PCL pair.

In interpretation of $T_{1\rho}{}^{H}$ data collected for PCL-rich compositions of MS > 7, special care should be exercised, regarding both CA- and CB-based copolymers; the plentiful PCL component in those samples provided two $T_{1\rho}{}^{H}$s, i.e., $T_{1\rho}{}^{H}_{fast}$ and $T_{1\rho}{}^{H}_{slow}$, due to development of the crystalline phase. In the case where CA was used as the trunk, the magnetization decay of the acetyl C2′ resonance yielded a $T_{1\rho}{}^{H}$ whose value almost coincided with that of another $T_{1\rho}{}^{H}$ from monitoring of the pyranose C2/C3/C5 signal, as demonstrated for $CA_{2.15}$-*g*-$PCL_{9.70}$ in Figure 2a. These values referring to the CA component were larger rather than those extrapolated from the other $T_{1\rho}{}^{H}$ data for the corresponding CA-*g*-PCLs of lower MS (< 3), but situated intermediate between $T_{1\rho}{}^{H}_{fast}$ and $T_{1\rho}{}^{H}_{slow}$ values referring to the crystallizable counter-component PCL. From these observations, we can deduce for the CA-based copolymers rich in PCL that the acetyl group is kept under firm restraint to the cellulose backbone, and the molecular mobility of the unified CA trunk is somewhat restricted by the contiguous PCL crystalline domains.

<< Figure 2 >>

In the case of CB-based copolymers of MS > 7, interestingly, the decay of the butyryl C4′ signal was characterized by two different $T_{1\rho}{}^{H}$ values, while that of the skeletal C2/C3/C5 signal provided a single $T_{1\rho}{}^{H}$; the specific behavior is exemplified for $CB_{2.10}$-*g*-$PCL_{9.03}$ in Figure 2b. Plainly, the shorter $T_{1\rho}{}^{H}$ and longer one quantified for the decayed butyryl C4′ resonance can be associated, respectively, with an amorphous phase and with an ordered phase, judging from comparison in magnitude with the other $T_{1\rho}{}^{H}$ data for the CB-*g*-PCL samples of the same butyryl DS. This observation enables us to infer that the butyryl substituent would be considerably free from restraint to the cellulose backbone and, partly, even intrude into the surface region of the PCL lamellar crystals; a similar suggestion has been given in the crystallization kinetic studies [5,6]. This accessibility would derive from the higher structural affinity of the (C6-O-)butyryl group of CB with a repeating unit of PCL [6].

3.2. Dynamic mechanical analysis

In order to detect the relaxation processes originating from the molecular motions of the copolymer constituents, DMA measurements were performed for different compositions of CA-*g*-PCLs and CB-*g*-PCLs. Figure 3 depicts the temperature dependence of the dynamic storage modulus E' and loss modulus E'' for $CA_{2.15}$-*g*-PCLs and $CB_{2.10}$-*g*-PCLs with different MSs. In both copolymer series, the E' plots make a curve of relatively simple configuration, but the E'' data are complicated by the presence of multiple dispersions.

<< Figure 3 >>

3.2.1. Assignments of relaxation processes for CEs and PCL homopolymer

Figure 4 shows E'' versus temperature plots on an enlarged scale for (a) $CA_{2.15}$-*g*-PCLs, (b) $CA_{2.98}$-*g*-PCLs, (c) $CB_{2.10}$-*g*-PCLs, (d) $CB_{2.93}$-*g*-PCLs, and their respective constituent polymers (CE_x and PCL). First, relaxation processes are assigned for CA, CB, and PCL homopolymer. In the data of the original CAs, four relaxation processes were observed, being labeled as α_{CA}, β_{CA}, γ_{CA1}, and γ_{CA2} from the higher temperature side (see Figure 4a and b, top). The principal α_{CA} relaxation appearing around 200 °C is associated with the glass transition, i.e., the micro-Brownian motions of the CA chains. The β_{CA} relaxation lying as a broad peak in a range 90–130 °C may be interpreted as due to moisture sorption [8,9]. However, the peak was quite feeble, and it was almost indiscernible in the DMA curves of the CA-based copolymers, reflecting that all the samples used in this work were well dried and repelled moisture. At lower temperatures from −150 to 25 °C, two peaks labeled as γ_{CA1} and γ_{CA2} were detected irrespective of the acetyl DS of the CAs used. The identification of these dispersions remains controversial. In literature, they are assigned to local motions of the repeating units (glucopyranose rings) [8,9,12,13], water combined with hydroxymethyl groups [8,9], or acetyl side-groups which would behave differently according to the substituted position [10,12]. Considering the prevalence of little moisture absorption in the present CA samples, the second possibility can be excluded. According to a trusty study on dielectric properties of cellulose and its derivatives including CA [12], it would be rather reasonable to assign the γ_{CA1} and γ_{CA2} processes to the acetyl motion at C2/C3 and that at C6, respectively. Then, an oscillatory fluctuation of glucopyranose rings strung via β(1-4) linkage [12] might have overlapped with the two γ-processes, but the situation was not signalized in any of the E'' data.

<< Figure 4 >>

In the case of CB, as shown in Figure 4c (top), a small E'' peak designated as δ_{CB} was perceived around −150 °C, in addition to α_{CB}, β_{CB}, γ_{CB1}, and γ_{CB2} corresponding to the four relaxations mentioned above for CA. The δ_{CB} process can be ascribed to a slight motion of the alkyl sequence in the butyryl side-groups [10,13]. As to PCL homopolymer, the film sample exhibited three processes (e.g., Figure 4c, bottom): β_{PCL} process (ca. −135 °C) attributed to a local crankshaft-type motion in the amorphous and crystalline regions [22]; α_{PCL} process (ca. −40 °C) associated with the micro-Brownian motion accompanying the amorphous glass transition; and fusion of PCL crystals, taking place at ~50 °C that agrees with T_m (= 52 °C) estimated by DSC.

3.2.2. Composition dependence of relaxation behavior for CE-g-PCLs

In Figure 4, T_g data obtained by DSC are also shown for the samples used for the DMA study, the temperature position being marked by an arrow on the respective E'' curves. From the T_g data and the result of $T_{1\rho}{}^{H}$ measurements, the $CA_{2.15}$-, $CB_{2.10}$-, and $CB_{2.93}$-based copolymer samples were assumed to form an amorphous phase in which the trunk and graft components were homogeneously mixed at the level of a few nanometers, but this was not applicable to the $CA_{2.98}$-based samples. Here, our major concern for the copolymer series is how the principal α_{CE} (α_{CA} or α_{CB}) and α_{PCL} signals vary with the composition as a function of MS.

In Figure 4a, we can find the largest dispersion signal (α) located at a temperature position near T_g for any composition of the $CA_{2.15}$-based copolymers. However, another prominent peak can also be found below or above T_g, labeled as α'_{PCL} for the CA-rich compositions of MS < 1 and similarly as α'_{CA} for the compositions of MS = 1–2.5. As indicated by dotted lines, plainly, the peak positions of α'_{CA} and α'_{PCL} are continuous with the original α_{CA} and α_{PCL} positions, respectively, and hence the former two relaxations can be regarded as being essentially commensurate with the latter reflecting the micro-Brownian motions of the CA and PCL chain segments. Similar observations were made for $CA_{2.45}$-based copolymer samples (data not shown). Thus, in these CA-*g*-PCL samples under mechanical oscillation, the linked CA and PCL components behave with still mutually different chain-segmental dynamics, despite the better mixing homogeneity in the scale of a few nanometers.

For $CA_{2.98}$-*g*-PCL copolymers (Figure 4b), we can see the samples of MS > 2 providing

two large dispersions assigned as α_{CA} (ca. 145 °C) and α_{PCL} (−40 °C). This observation is natural, because the two T_gs originating from phase-separated CA and PCL domains were already detected by DSC, as arrowed at ca. 160 and −55 °C, respectively. In a data for a sample of MS = 0.55, there occurs α'_{PCL} below T_g in addition to α_{CA}, similar to the situation for $CA_{2.15}$-*g*-PCLs rich in CA.

Dynamic heterogeneity was also found for the CB-*g*-PCL series. As illustrated in Figure 4c and d, two principal dispersions to be labeled as α'_{CB} and α'_{PCL} are distinguishable in the E'' data of $CB_{2.10}$-*g*-$PCL_{0.60}$ and $CB_{2.93}$-*g*-$PCL_{0.50}$. However, these copolymer samples of MS ≈ 0.5–0.6 gave a calorimetric T_g just intermediate between the α'_{CB} and α'_{PCL} locations, such a behavior being never experienced with the CA-g-PCL series. Additionally, irrespective of the butyryl DS, the α'_{CB} signal was not clearly observed for the CB-based copolymers having longer PCL side-chains of MS > 2, and, reversely, at the compositions of MS < 0.5, the richer component CB dominated the primary relaxation process of the copolymers. This tendency of assimilation was more prominent in the CB-based series.

Regarding the local relaxations appearing below −50 °C, we found no significant shift of the corresponding E''-peaks for any of the CA- and CB-based copolymer series. Generally, the β_{PCL} peak became more pronounced with increasing MS, and the γ_{CA2} and γ_{CB2} peaks became suppressed with MS, with their temperature positions almost unchanged. However, the CA-based series, rather than the CB-based one, exhibited both of the two local relaxation signals in a much wider range of MS, as can be seen in Figure 4a; the β_{PCL} process was signalized even for the copolymer sample of MS = 0.27 and the γ_{CA2} one still remained in the sample of MS = 2.50.

3.3. Dielectric relaxation analysis

Dielectric relaxation spectroscopy, DRS, is a useful method for investigating molecular dynamics of polymer materials in a widely extended time scale, if the moving sites of the repeating unit and the attached side-groups own a permanent dipole moment. In the present CE-*g*-PCL systems, any of the constituents has a dielectrically active site: -C-O-C- in the cellulose backbone chain and C=O in the acyl groups and PCL side-chains. DRS can also provide information about distribution of the relaxation time referring to a molecular motion considered. In this work, we carried out DRS measurements for the two CE-*g*-PCL series, with the purpose of elucidating a possible cooperativeness in the two segmental motions of

the CE trunk- and PCL side-chains and clarifying the difference in the extent between the CA-based series and the CB-based one.

DRS spectra are generally described in a combination form of the real (ε') and imaginary (ε'') parts of a complex dielectric function, but, in this paper, ε'' is entirely used for discussion. Figure 5 illustrates a few typical data of ε'', obtained for three copolymer samples based on CA. As far as the CA-based series was concerned, the relaxation processes observed in the DMA study were mostly detectable as parallels in the present DRS measurements. Regarding the principal amorphous relaxation (α) behavior, which is our prime concern, $CA_{2.15}$-*g*-PCL and $CA_{2.45}$-*g*-PCL samples of MS = 0.5–2.5 showed surely two discrete signals: α'_{PCL} and α_{CA} for the compositions of MS = 0.5–1.2, and α_{PCL} and α'_{CA} for those of MS = 1.3–2.5, using the same notations as in the DMA study. However, the α_{CA} and α'_{CA} relaxation processes were observed as a peak signal partly overlapping with an ascent of direct current (dc) conductivity (see Figure 5b and c). Concerning the CB-based graft series, somewhat surprisingly, only a single α relaxation, designated conventionally as α_{PCL} or α_{CB}, was observed and neither the α'_{CB} nor α'_{PCL} process was detected for any of the copolymer compositions in the DRS measurements.

<< Figure 5 >>

The relaxation processes detected as a discrete dispersion (e.g., α_{PCL} in Figure 5a) were simulated by using the following Havriliak-Negami equation [23]:

$$\varepsilon^* = \varepsilon_\infty + (\varepsilon_s - \varepsilon_\infty) / \left\{1 + (i\omega\tau)^{\beta_i}\right\}^{\alpha_i} \quad (4)$$

where ε_∞ and ε_s denote the limits to higher and lower frequencies, respectively, of the real component ε' of the complex permittivity ε^*; ω is the angular frequency of measurement, i.e., $\omega = 2\pi f$; τ is the dielectric relaxation time; and α_i and β_i are parameters that characterize the shape of the relaxation time distribution ($0 < \beta_i \leq 1$, $0 < \alpha_i\beta_i \leq 1$). In the present study, $\alpha_i = 1$, that is, a symmetrical Cole-Cole relationship [24], was assumed in estimation of the relaxation time distribution. Concerning the dispersion signals that overlapped with the dc conductivity, i.e., the α_{CA}, α'_{CA} and α_{CB} processes, the following equation including a correction term (the third one in the right side) was adopted to extract the respective relaxation processes:

$$\varepsilon^* = \varepsilon_\infty + (\varepsilon_s - \varepsilon_\infty) / \left\{1 + (i\omega\tau)^{\beta_i}\right\}^{\alpha_i} - i(\sigma_{dc}/\omega\varepsilon_0) \quad (5)$$

where σ_{dc} and ε_0 are the dc conductivity and the permittivity of vacuum, respectively.

Eventually, the major parameters of dielectric relaxation, τ and β_i, were successfully determined by application of Equation (4) or (5) with $\alpha_i = 1$ to the respective DRS data.

Figure 6 illustrates logarithmic plots of τ against the reciprocal of temperature (T^{-1}) for the α (and α′) processes of $CA_{2.15}$-*g*-PCL and $CB_{2.10}$-*g*-PCL samples with various compositions. In general, temperature dependence of τ for the primary α process involved in the micro-Brownian motion of polymer chains may be expressed by the following Vogel-Fulcher-Tammann (VFT) equation [25–27]:

(6)

where τ_0 is a pre-exponential factor, B is an activation parameter, and T_0 is a so-called Vogel temperature at which the main-chain motions are virtually frozen. Broken lines in Figure 6 indicate data fitting to the VFT equation. For the sake of convenience, an apparent activation energy E_a for the α and α′ processes was evaluated by Arrhenius approximation of the respective ln τ vs T^{-1} data to a linear regression in the range of the measurement. The values thus obtained are collected in Table 3 for all the copolymer samples explored.

<< Figure 6 >>

<< Table 3 >>

As can be seen from Figure 6a, τ values of the α_{CA} and α'_{CA} processes detected for the $CA_{2.15}$-based samples of MS ≤ 2.5 were all located in a range of −2 to 2 on the logarithmic scale. This implies that the mobility of the CA trunk chain was not drastically affected in time scale by the introduction of the oxycaproyl units. However, the emerging position of the relaxations shifted to the low temperature side systematically with an increase in MS and the activation energy E_a associated with the α_{CA} or α'_{CA} process also decreased with increasing MS (see Table 3). Similar tendencies were observed for the $CA_{2.45}$-*g*-PCL series. Thus it is certain that these CA trunks are enabled to undergo the micro-Brownian motion on heating at lower temperatures and more easily by the grafting with PCL chains.

In Figure 6a, when the data is viewed from the side of the PCL component, the process detected as α_{PCL} or α'_{PCL} shifts more or less to the positions of higher temperature and longer relaxation time as the MS decreases; this was also applicable to the $CA_{2.45}$-based copolymers concerned. It is therefore readily found that the molecular motion of the PCL side-chains partially involved the motion of the respective CA backbone chains. In other words, the motions of PCL units adjacent to the cellulose backbone were somewhat restricted due to the

anchoring onto the semi-rigid skeletal chain. In these CA-based series of DS = 2.15 and 2.45, a comparatively larger E_a of the α_{PCL} process was estimated only for the copolymers of MS = 1.2–2.5, as shown in Table 3. Evidently, there was no systematic dependence in value of E_a of the α_{PCL} process on the copolymer composition. For instance, samples of $CA_{2.15}$-*g*-$PCL_{9.70}$ and $CA_{2.45}$-*g*-$PCL_{9.30}$ provided a considerably small E_a value. In the copolymers of so high MSs, the anchoring effect on the segmental motion of the PCL side-chains may be rather inactive, which would allow the polyester side-chains to behave like a homopolymer of relatively low molecular weight. In the use of the $CA_{2.98}$-based series, deservedly, we observed the α_{PCL} process of generally low E_a, because of the trend of definite phase-separation of the two components.

On the other hand, the single α relaxation (α_{CB} or α_{PCL}) observed for the CB-based series shifted to the side of lower T and shorter τ at a noticeable rate with increasing MS in the ln τ vs T^{-1} plots, as exemplified in Figure 6b. Differing from the situation in the CA-based graft series, the range of ln τ observed for the α_{CB} process dropped sharply with a small increase in MS, e.g., ln $\tau \approx$ 1.5–3 for $CB_{2.10}$ and −3.5–1.5 for $CB_{2.10}$-*g*-$PCL_{0.60}$. Additionally, E_a required for the α_{CB} process reduced in almost inverse proportion to MS, so that the values connected smoothly with the corresponding data for the α_{PCL} process; this was a common observation irrespective of the butyryl DS of the CB trunk adopted (see Table 3). It should also be noted that an E_a value estimated for the PCL-richest sample (W_{PCL} > ~75 wt%) in the respective CB-based series was always larger than that for the corresponding CA-based one having a comparable acyl DS. These results may be interpreted as due to a higher cooperation in segmental motions between the CB trunk- and PCL side-chains, suggesting the generally better homogeneity in the film samples of the CB-*g*-PCL series, as well.

Figure 7 shows a result of the determination of β_i appearing in Equation (4) and (5) for the α (and α′) processes of $CA_{2.15}$-*g*-PCLs and $CB_{2.10}$-*g*-PCLs, the data being plotted as a function of the PCL content W_{PCL}. Generally, this kind of parameter is a measure indicating the degree of distribution of the relaxation time associated with a considered molecular dynamic process; viz., a value of β_i = 1 means that there occurs just a single relaxation mode, while, in contrast, when the width of the distribution is rather broad due to coexistence of many relaxation modes in the process, the parameter assumes a much smaller value to approach zero. As can be seen from Figure 7a, β_i values for the α_{CA} and α'_{CA} processes of

the CA-based copolymers were almost equal to that (~0.82) for α_{CA} of the original CA, irrespective of the PCL weight content. Similarly, the α_{PCL} and α'_{PCL} processes kept β_i almost constant at ~0.3. These observations of β_i values remaining unchanged regardless of the grafted PCL amount would reflect a poor correlation in chain-segmental dynamics between the CA and PCL components.

<< Figure 7 >>

In the other graft series $CB_{2.10}$-*g*-PCLs (Figure 7b), β_i values for the α_{CB} and α_{PCL} processes were both inclined to diminish with an increase of W_{PCL}, indicating that the distribution of the relaxation time in the two α processes became more broadened with increasing PCL content. It can therefore be reasonably assumed that the segmental motion of the CB trunk-chain and that of the PCL side-chains correlated with each other to a considerable extent. Such a higher cooperativeness between the two components implies a more reduced dynamic heterogeneity in the CB-based copolymer films, unlike the situation in the CA-based graft series.

4. Conclusions

The authors performed solid-state structural characterization for two CE-based graft copolymer series, CA-*g*-PCLs and CB-*g*-PCLs, through observations of the nuclear magnetic, dynamic mechanical, and dielectric relaxation behavior. The samples of both series were prepared with acyl DSs of ~2.1, ~2.5, and ~2.95 to assume various compositions, typically, oxycaproyl MS ≈ 0.15–9.0.

Except for virtually block-like $CA_{2.98}$-*g*-PCLs, all the other copolymers formed a homogeneous amorphous phase in which the trunk and graft components were mixed well at the level of a few nanometers, as confirmed by the result of $T_{1\rho}{}^{H}$ measurements in ^{13}C NMR spectroscopy in addition to the T_g data in the preliminary DSC study. In both CE-based series, however, the PCL component introduced at MS > 7 was allowed to develop a crystalline phase when the copolymer concerned was cooled from the molten sate. An important conclusion based on the $T_{1\rho}{}^{H}$ quantifications is that the butyryl substituent in the CB-based copolymers would be fairly free from restraint to the cellulose backbone, while the acetyl group in the CA-based ones is kept under firm restraint to the backbone.

In DMA measurements, the two CE-based copolymer series gave, more or less, a response of dynamic heterogeneity; i.e., the semi-rigid CE and flexible PCL components

behaved with mutually different chain-segmental dynamics, despite the compulsory linkage and the assurance of good mixing on the dimensional scale of a few nanometers. Regarding the extent of cooperativeness between the CE trunk- and PCL side-chains, a decisive solution was acquired by DRS measurements; viz., the segmental motions of the two components in the CB-based copolymers were more cooperative with each other, relative to the situation in the CA-based ones. This conclusion was drawn based on comparison of the composition dependence of the relaxation time, the activation energy, the degree of relaxation time distribution for the principal α processes, between the two CE-based copolymer series. Probably, the butyryl substituent, having a higher structural affinity with a repeating unit of the PCL side-chain, would act as internal compatibilizer to reduce dynamic heterogeneity in the CB-based copolymer samples.

References

[1] Edgar KJ, Buchanan CM, Debenham JS, Rudquist PA, Seiler BD, Shelton MC, Tindall D. Prog Polym Sci 2001;26:1605–1688.

[2] Klemm D, Heublein B, Fink HP, Bohn A. Angew Chem Int Ed 2005;44:3358–3393.

[3] Nishio Y. Adv Polym Sci 2006;205:97–151.

[4] Teramoto Y, Nishio Y. Biomacromolecules 2004;5:407–414.

[5] Kusumi R, Teramoto Y, Nishio Y. Macromol Chem Phys 2008;209:2135–2146.

[6] Kusumi R, Inoue Y, Shirakawa M, Miyashita Y, Nishio Y. Cellulose 2008;15:1–16.

[7] Kusumi R, Lee SH, Teramoto Y, Nishio Y. Biomacromolecules 2009;10:2830–2838.

[8] Scandola M, Ceccorulli G. Polymer 1985;26:1953–1957.

[9] Pizzoli M, Scandola M, Ceccorulli G. Viscoelastic relaxations of cellulose acetate in the solid-state. In: Kennedy JF, Phillips GO, Williams PA, editors. Wood and Cellulosics: Industrial Utilization, Biotechnology, Structure and Properties, Chichester: Ellis Horwood Limited, 1987. pp. 105–110.

[10] Morooka T, Norimoto M, Yamada T, Shiraishi N. Wood Res 1983;69:61–70.

[11] Crofton DJ, Moncrieff D, Pethrick RA. Polymer 1982;23:1605–1608.

[12] Einfeldt J, Meißner D, Kwasniewski A. Prog Polym Sci 2001;26:1419–1472.

[13] Seymour RW, Weinhold S, Haynes SK. J Macromol Sci -Phys 1979;B16:337–353.

[14] Hatakeyama H, Yoshida T, Hatakeyama T. J Therm Anal Cal 2000;59:157–168.

[15] Vidéki B, Klébert S, Pukánszky B. J Polym Sci Part B Polym Phys 2007;45:873–883.

[16] Számel G, Klébert S, Sajó I, Pukánszky B. J Therm Anal Cal 2008;91:715–722.

[17] Teramoto Y, Ama S, Higeshiro T, Nishio Y. Macromol Chem Phys 2004;205:1904–1915.

[18] Ohno T, Yoshizawa S, Miyashita Y, Nishio Y. Cellulose 2005;12:281–291.

[19] Ohno T, Nishio Y. Cellulose 2006;13:245–259.

[20] Huang JM, Yang SJ. Polymer 2005;46:8068–8078.

[21] McBrierty VJ, Douglass DC. J Polym Sci Macromol Rev 1981;16:295–366.

[22] Grimau M, Laredo E, Pérez MCY, Bello A. J Chem Phys 2001;114:6417–6425.

[23] Havriliak S, Negami S. Polymer 1967;8:161–210.

[24] Cole KS, Cole RH. J Chem Phys 1941;9:341–351.

[25] Vogel H. Phys Z 1921;22:645–646.

[26] Fulcher GS. J Am Ceram Soc 1925;8:339–355.

[27] Tammann G, Hesse W. Z Anorg Allg Chem 1926;156:245–257.

Figure Captions

Figure 1. Solid-state ^{13}C CP/MAS NMR spectra for $CA_{2.15}$, $CA_{2.15}$-*g*-$PCL_{9.70}$, plain PCL, $CB_{2.10}$-*g*-$PCL_{9.03}$, and $CB_{2.10}$, and their peak assignments. Asterisks denote a spinning sideband overlapping with a resonance signal of C4 pyranose carbon. The C2″ peak for $CB_{2.10}$-*g*-$PCL_{9.03}$ contains a small intensity of C2′ of the butyryl substituent.

Figure 2. Semilogarithmic plots of the decay of ^{13}C resonance intensities as a function of spin-locking time *t*, for film samples of (a) $CA_{2.15}$-*g*-$PCL_{9.70}$ and (b) $CB_{2.10}$-*g*-$PCL_{9.03}$. Straight lines indicate the fitting to a single exponential function (see Equation 1) for acetyl C2′ of $CA_{2.15}$-*g*-$PCL_{9.70}$ and pyranose C2/C3/C5 of $CA_{2.15}$-*g*-$PCL_{9.70}$ and $CB_{2.10}$-*g*-$PCL_{9.03}$. Dashed-line curves indicate the fitting to a double exponential function (see Equation 2) with $x_f = 0.34$ and $x_s = 0.66$ for PCL side-chain C5″ of $CA_{2.15}$-*g*-$PCL_{9.70}$; $x_f = 0.82$ and $x_s = 0.18$ for butyryl C4′ of $CB_{2.10}$-*g*-$PCL_{9.03}$; and $x_f = 0.32$ and $x_s = 0.68$ for PCL side-chain C5″ of $CB_{2.10}$-*g*-$PCL_{9.03}$.

Figure 3. Temperature dependence of the dynamic storage modulus E' and loss modulus E'' for (a) $CA_{2.15}$-*g*-PCLs and (b) $CB_{2.10}$-*g*-PCLs with different MSs. The oscillatory frequency of the measurement was 10 Hz.

Figure 4. E'' versus temperature plots on an enlarged scale for CEs, PCL, and CE-*g*-PCLs: (a) $CA_{2.15}$-*g*-PCLs; (b) $CA_{2.98}$-*g*-PCLs; (c) $CB_{2.10}$-*g*-PCLs; (d) $CB_{2.93}$-*g*-PCLs. The E'' data (obtained at 10 Hz) are displaced vertically by ~1.0 log unit, relative to the normal position for PCL as reference. Numerals (*y*) indicate a value of MS for each copolymer sample. Arrows indicate a T_g position taken as the midpoint of a baseline shift appearing in DSC heat flow.

Figure 5. Dielectric loss ε'' curves of the relaxation processes: (a) α_{PCL} process for $CA_{2.15}$-*g*-$PCL_{9.70}$; (b) α_{CA} process for $CA_{2.15}$-*g*-$PCL_{0.27}$; (c) α'_{CA} process for $CA_{2.15}$-*g*-$PCL_{2.50}$.

Figure 6. Logarithmic plots of the relaxation time τ against the reciprocal of absolute temperature for (a) α and α' processes of $CA_{2.15}$-*g*-PCLs and (b) α process of $CB_{2.10}$-*g*-PCLs.

Broken-line curves indicate data fitting to the VFT equation.

Figure 7. Parameter β_i charactering the degree of relaxation time distribution, plotted as a function of the PCL weight content W_{PCL} for (a) α and α′ processes of $CA_{2.15}$-*g*-PCLs and (b) α process of $CB_{2.10}$-*g*-PCLs.

Table 1 Composition parameters, molecular weights, and thermal transition data for CAs, CBs, PCL, CA-*g*-PCLs, and CB-*g*-PCLs examined in the present study.

Samples	acyl DS	MS	DP_s'	W_{PCL} /wt%	M_w [a] /kg·mol^{-1}	M_n [a] /kg·mol^{-1}	M_w/M_n [a]	T_g /°C	T_m /°C
$CA_{2.15}$ [b]	2.15	–	–	–	134	52.4	2.56	204	n.d. [d]
$CA_{2.45}$ [b]	2.45	–	–	–	152	51.5	2.95	192	n.d.
$CA_{2.98}$ [b]	2.98	–	–	–	128	30.4	4.21	175	295
$CB_{2.10}$	2.10	–	–	–	827	323	2.56	129	n.d.
$CB_{2.50}$	2.50	–	–	–	621	305	2.04	118	n.d.
$CB_{2.93}$ [b]	2.93	–	–	–	907	404	2.25	98.3	n.d.
PCL [c]	–	–	–	100	56.5	22.4	2.52	−61.2	51.9
$CA_{2.15}$-*g*-$PCL_{0.27}$	2.15	0.27	0.32	10.9	151	73.0	2.07	141	n.d.
$CA_{2.15}$-*g*-$PCL_{0.87}$	2.15	0.87	1.02	28.3	168	56.9	2.95	97.3	n.d.
$CA_{2.15}$-*g*-$PCL_{1.30}$	2.15	1.30	1.53	37.1	202	63.5	3.18	−25.0	n.d.
$CA_{2.15}$-*g*-$PCL_{2.50}$ [c]	2.15	2.50	2.94	52.9	226	124	1.82	−28.3	n.d.
$CA_{2.15}$-*g*-$PCL_{9.70}$ [c]	2.15	9.70	11.4	81.4	384	191	2.01	−57.2	38.3
$CA_{2.45}$-*g*-$PCL_{0.11}$	2.45	0.11	0.20	4.53	177	81.7	2.17	163	n.d.
$CA_{2.45}$-*g*-$PCL_{0.22}$	2.45	0.22	0.40	8.67	193	85.4	2.26	172	n.d.
$CA_{2.45}$-*g*-$PCL_{1.20}$	2.45	1.20	2.18	34.1	249	108	2.31	85.5	n.d.
$CA_{2.45}$-*g*-$PCL_{2.50}$	2.45	2.50	4.55	51.9	252	136	1.85	−42.0	n.d.
$CA_{2.45}$-*g*-$PCL_{9.30}$	2.45	9.30	16.9	80.0	452	184	2.46	−59.5	42.2
$CA_{2.98}$-*g*-$PCL_{0.22}$	2.98	0.22	11.0	8.03	139	40.3	3.45	156	283
$CA_{2.98}$-*g*-$PCL_{0.55}$	2.98	0.55	27.5	17.9	146	38.0	3.84	135	274
$CA_{2.98}$-*g*-$PCL_{2.07}$ [c]	2.98	2.07	104	45.1	1880	743	2.52	−54.8	n.d.
$CA_{2.98}$-*g*-$PCL_{9.20}$ [b]	2.98	9.20	460	78.5	5050	2660	1.90	168 −59.0 163	258 49.5 259
$CB_{2.10}$-*g*-$PCL_{0.16}$	2.10	0.16	0.18	5.59	1200	510	2.35	124	n.d.
$CB_{2.10}$-*g*-$PCL_{0.60}$	2.10	0.60	0.67	18.2	1620	672	2.41	34.8	n.d.
$CB_{2.10}$-*g*-$PCL_{2.33}$ [c]	2.10	2.33	2.59	46.3	2090	893	2.34	−46.3	n.d.
$CB_{2.10}$-*g*-$PCL_{9.03}$ [c]	2.10	9.03	10.0	77.0	3750	1640	2.29	−57.4	48.0
$CB_{2.50}$-*g*-$PCL_{0.26}$	2.50	0.26	0.52	8.10	690	312	2.21	106	n.d.
$CB_{2.50}$-*g*-$PCL_{1.37}$	2.50	1.37	2.74	31.7	834	365	2.28	−18.1	n.d.
$CB_{2.50}$-*g*-$PCL_{3.49}$	2.50	3.49	6.98	54.2	2720	1210	2.25	−42.3	n.d.
$CB_{2.50}$-*g*-$PCL_{7.42}$	2.50	7.42	14.8	71.5	3900	1750	2.23	−55.1	48.5
$CB_{2.93}$-*g*-$PCL_{0.23}$	2.93	0.23	3.29	6.67	1160	495	2.34	87.4	n.d.
$CB_{2.93}$-*g*-$PCL_{0.50}$	2.93	0.50	7.14	13.4	1660	601	2.76	17.3	n.d.
$CB_{2.93}$-*g*-$PCL_{3.58}$ [c]	2.93	3.58	51.1	52.6	2700	1340	2.02	−38.2	n.d.
$CB_{2.93}$-*g*-$PCL_{12.6}$ [b]	2.93	12.6	180	79.6	7070	3650	1.94	−54.4	51.3

[a] Determined by gel permeation chromatography (mobile phase, 0.25 mL·min^{-1} tetrahydrofuran at 40°C) with polystyrene standards. [b] Quoted from ref [5]. [c] Quoted from ref [7]. [d] Could not be detected.

Table 2 $T_{1\rho}{}^{H}$ Data for CEs, PCL, and CE-*g*-PCLs.

Samples	$T_{1\rho}{}^{H}$ /ms			
	CA or CB component		PCL component	
	Pyranose C2C3C5	Acetyl C2′ or Butyryl C4′	C3″C4″	C5″
$CA_{2.15}$	13.7	13.9	–	–
$CA_{2.15}$-*g*-$PCL_{0.27}$	12.9	13.3	12.8	12.3
$CA_{2.15}$-*g*-$PCL_{0.87}$	8.46	7.87	8.02	8.30
$CA_{2.15}$-*g*-$PCL_{1.30}$	6.99	7.11	4.72	3.72
$CA_{2.15}$-*g*-$PCL_{2.50}$	2.79	2.74	2.20	1.71
$CA_{2.15}$-*g*-$PCL_{9.70}$	4.05	3.79	3.01[a] / 24.3[b]	3.63[a] / 24.6[b]
$CA_{2.45}$	16.6	15.9	–	–
$CA_{2.45}$-*g*-$PCL_{0.11}$	14.0	14.4	13.6	13.2
$CA_{2.45}$-*g*-$PCL_{0.22}$	11.4	11.7	9.03	7.23
$CA_{2.45}$-*g*-$PCL_{1.20}$	6.21	5.64	4.02	4.17
$CA_{2.45}$-*g*-$PCL_{2.50}$	3.02	2.68	2.05	2.39
$CA_{2.45}$-*g*-$PCL_{9.30}$	7.49	8.31	4.10[a] / 22.5[b]	4.83[a] / 23.3[b]
$CA_{2.98}$	15.7	15.4	–	–
$CA_{2.98}$-*g*-$PCL_{0.22}$	13.7	13.9	8.95	9.03
$CA_{2.98}$-*g*-$PCL_{0.55}$	12.3	14.0	7.62	6.39
$CA_{2.98}$-*g*-$PCL_{2.07}$	6.34	5.64	3.49	4.52
$CA_{2.98}$-*g*-$PCL_{9.20}$	7.09	7.87	2.15[a] / 22.0[b]	1.75[a] / 21.6[b]
$CB_{2.10}$	9.20	8.64	–	–
$CB_{2.10}$-*g*-$PCL_{0.16}$	7.45	6.73	8.58	6.42
$CB_{2.10}$-*g*-$PCL_{0.60}$	6.58	6.23	6.47	5.23
$CB_{2.10}$-*g*-$PCL_{2.33}$	3.24	3.11	2.48	2.69
$CB_{2.10}$-*g*-$PCL_{9.03}$	3.94	2.02[a] / 18.0[b]	3.86[a] / 27.3[b]	3.00[a] / 31.1[b]
$CB_{2.50}$	7.60	7.90	–	–
$CB_{2.50}$-*g*-$PCL_{0.26}$	7.09	7.26	n.d.[c]	n.d.
$CB_{2.50}$-*g*-$PCL_{1.37}$	3.89	3.23	3.45	n.d.
$CB_{2.50}$-*g*-$PCL_{3.49}$	3.26	3.50	3.96	3.55
$CB_{2.50}$-*g*-$PCL_{7.42}$	4.82	3.20[a] / 18.3[b]	3.68[a] / 29.4[b]	4.83[a] / 31.6[b]
$CB_{2.93}$	8.26	7.60	–	–
$CB_{2.93}$-*g*-$PCL_{0.23}$	7.73	7.67	n.d.	n.d.
$CB_{2.93}$-*g*-$PCL_{0.50}$	5.81	5.36	n.d.	n.d.
$CB_{2.93}$-*g*-$PCL_{3.58}$	3.25	2.80	3.64	3.00
$CB_{2.93}$-*g*-$PCL_{12.6}$	n.d.	3.12[a] / 18.7[b]	7.20[a] / 35.0[b]	7.29[a] / 38.0[b]
PCL	–	–	6.29[a] / 60.2[b]	7.17[a] / 61.8[b]

[a] $T_{1\rho}{}^{H}_{fast}$. [b] $T_{1\rho}{}^{H}_{slow}$. [c] Could not be detected.

Table 3 Activation energy E_a for the dielectric α relaxation processes of CEs, PCL, and CE-*g*-PCLs.

Samples	α_{CA} or α_{CB} /kJ·mol^{-1}	α_{PCL} /kJ·mol^{-1}
$CA_{2.15}$	167	–
$CA_{2.15}$-*g*-$PCL_{0.27}$	102	n.d.[a)]
$CA_{2.15}$-*g*-$PCL_{0.87}$	97.2	15.7[b)]
$CA_{2.15}$-*g*-$PCL_{1.30}$	98.6[c)]	45.3
$CA_{2.15}$-*g*-$PCL_{2.50}$	71.4[c)]	65.9
$CA_{2.15}$-*g*-$PCL_{9.70}$	n.d.	18.2
$CA_{2.45}$	243	–
$CA_{2.45}$-*g*-$PCL_{0.11}$	190	n.d.
$CA_{2.45}$-*g*-$PCL_{0.22}$	97.8	n.d.
$CA_{2.45}$-*g*-$PCL_{1.20}$	91.0	45.1[b)]
$CA_{2.45}$-*g*-$PCL_{2.50}$	70.5[c)]	66.5
$CA_{2.45}$-*g*-$PCL_{9.30}$	n.d.	29.3
$CA_{2.98}$	96.6	–
$CA_{2.98}$-*g*-$PCL_{0.22}$	70.3	n.d.
$CA_{2.98}$-*g*-$PCL_{0.55}$	n.d.	27.3[b)]
$CA_{2.98}$-*g*-$PCL_{2.07}$	76.9[c)]	25.6
$CA_{2.98}$-*g*-$PCL_{9.20}$	n.d.	12.5
$CB_{2.10}$	128	–
$CB_{2.10}$-*g*-$PCL_{0.16}$	145	n.d.
$CB_{2.10}$-*g*-$PCL_{0.60}$	135	n.d.
$CB_{2.10}$-*g*-$PCL_{2.33}$	n.d.	45.9
$CB_{2.10}$-*g*-$PCL_{9.03}$	n.d.	25.0
$CB_{2.50}$	200	–
$CB_{2.50}$-*g*-$PCL_{0.26}$	148	n.d.
$CB_{2.50}$-*g*-$PCL_{1.37}$	67.1	n.d.
$CB_{2.50}$-*g*-$PCL_{3.49}$	n.d.	58.0
$CB_{2.50}$-*g*-$PCL_{7.42}$	n.d.	32.9
$CB_{2.93}$	151	–
$CB_{2.93}$-*g*-$PCL_{0.23}$	122	n.d.
$CB_{2.93}$-*g*-$PCL_{0.50}$	119	n.d.
$CB_{2.93}$-*g*-$PCL_{3.58}$	n.d.	82.6
$CB_{2.93}$-*g*-$PCL_{12.6}$	n.d.	33.0
PCL	–	31.2

[a)] Could not be detected. [b)] Estimated for α'_{PCL} process. [c)] Estimated for α'_{CA} process.

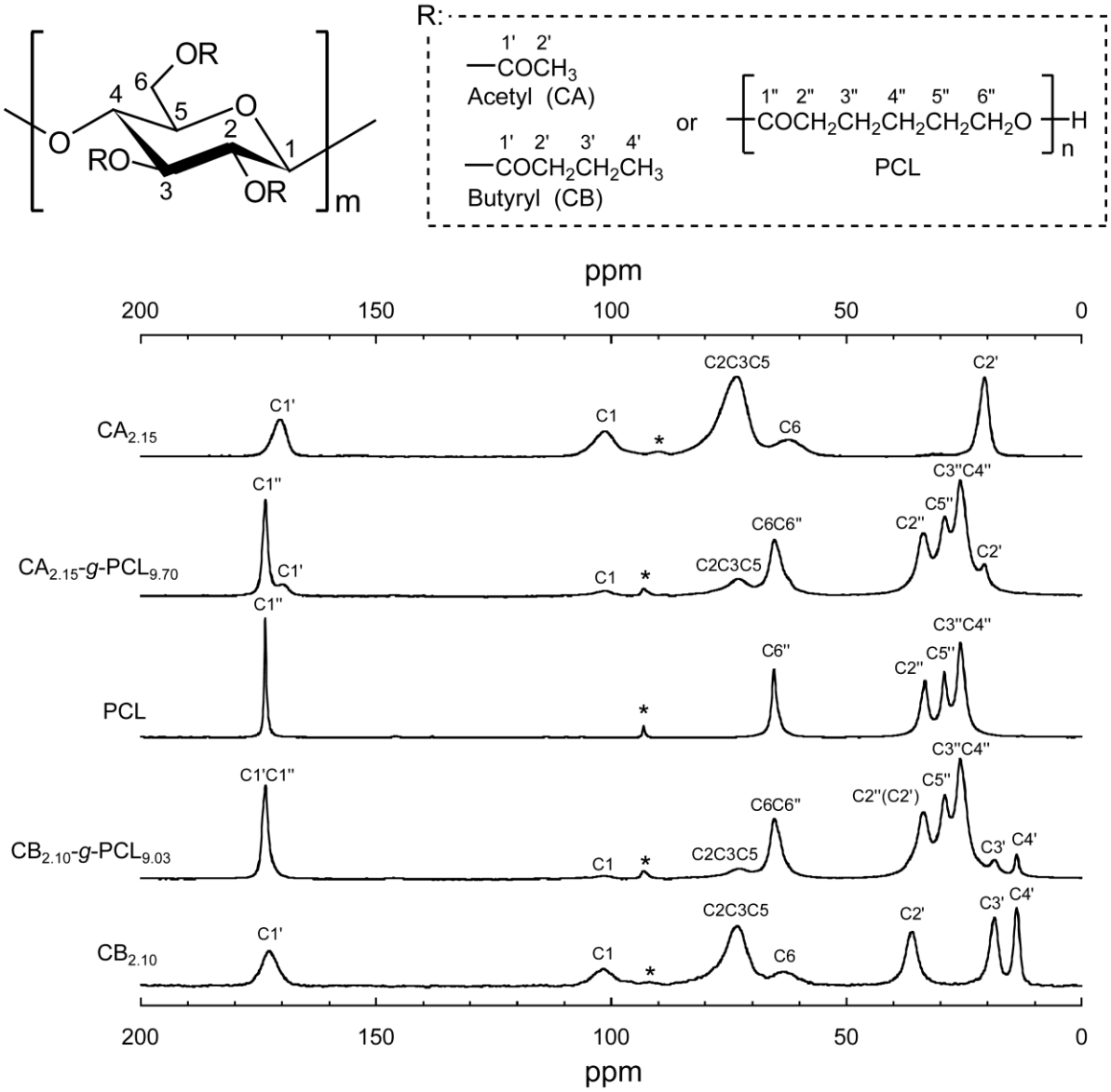

Figure 1.

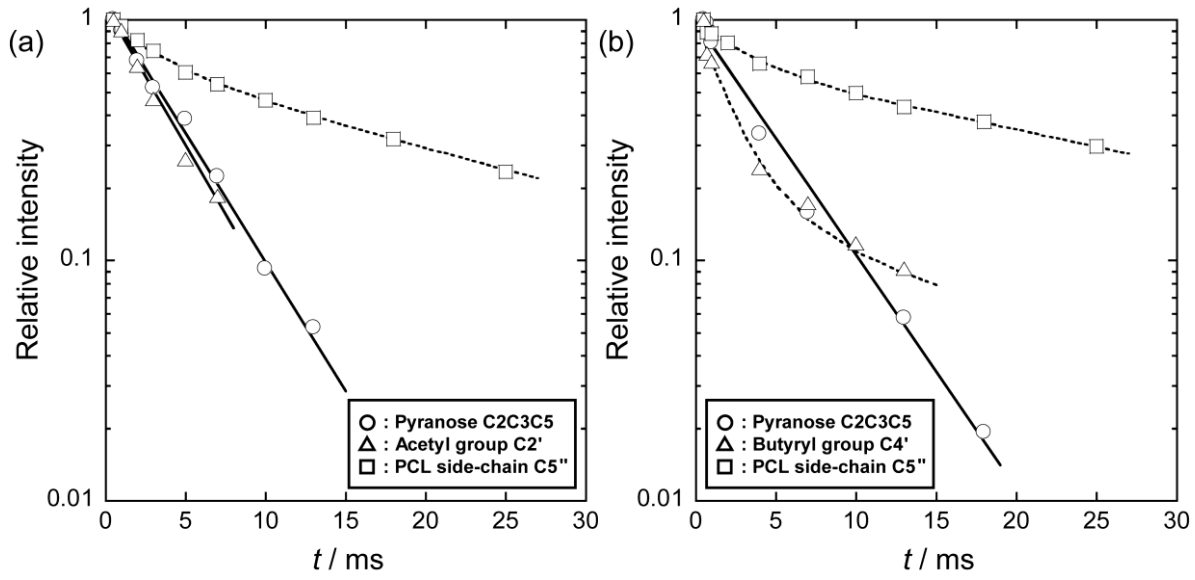

Figure 2.

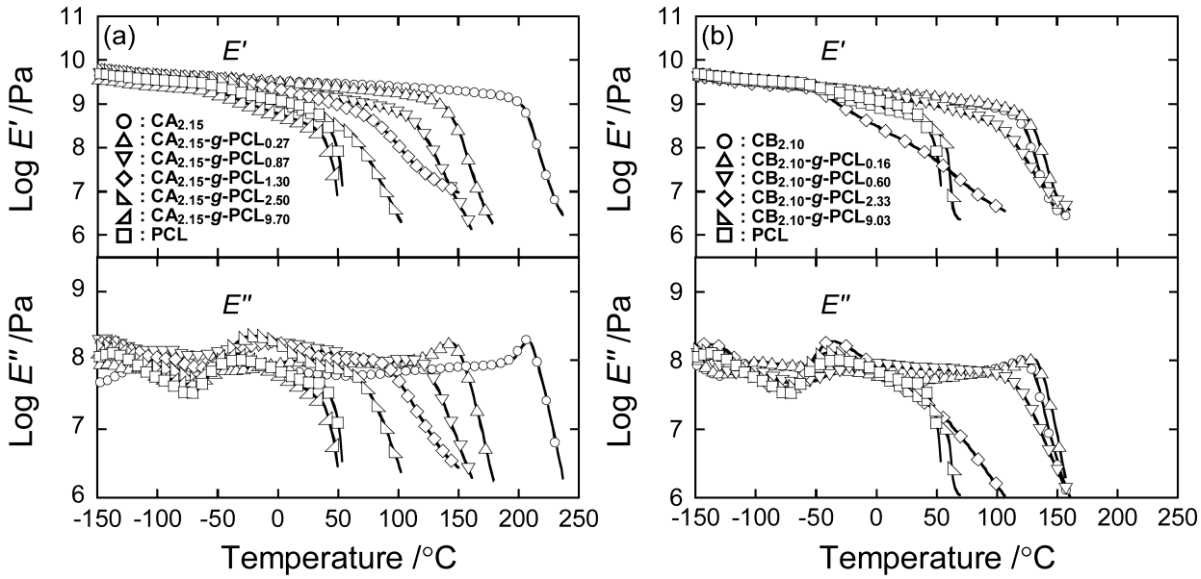

Figure 3.

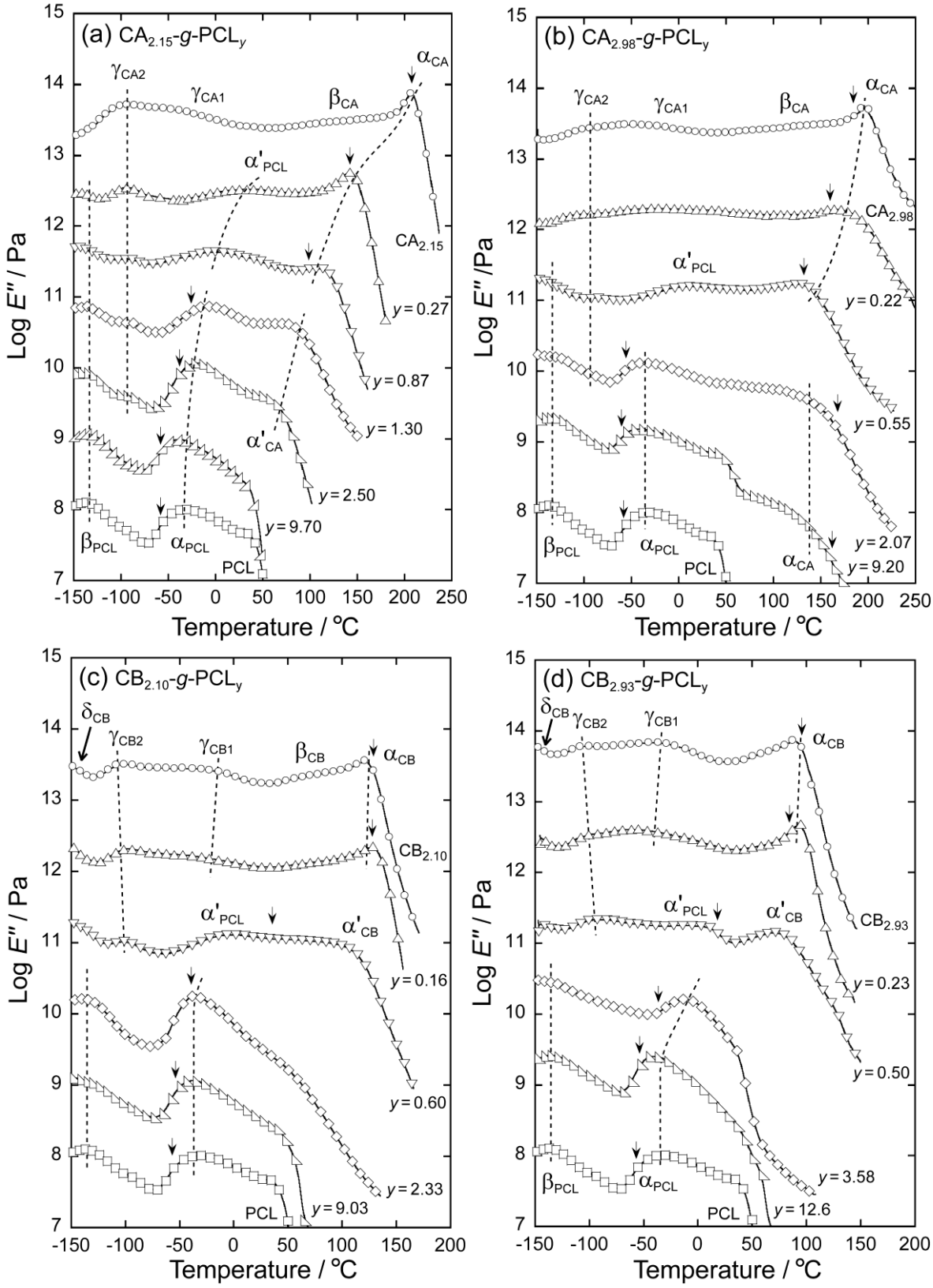

Figure 4.

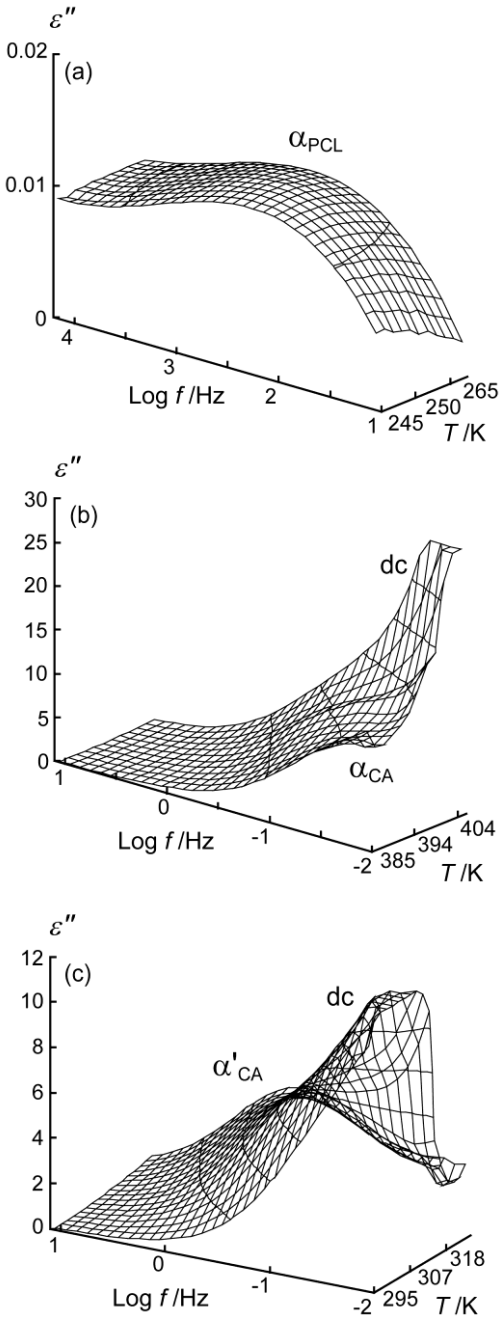

Figure 5.

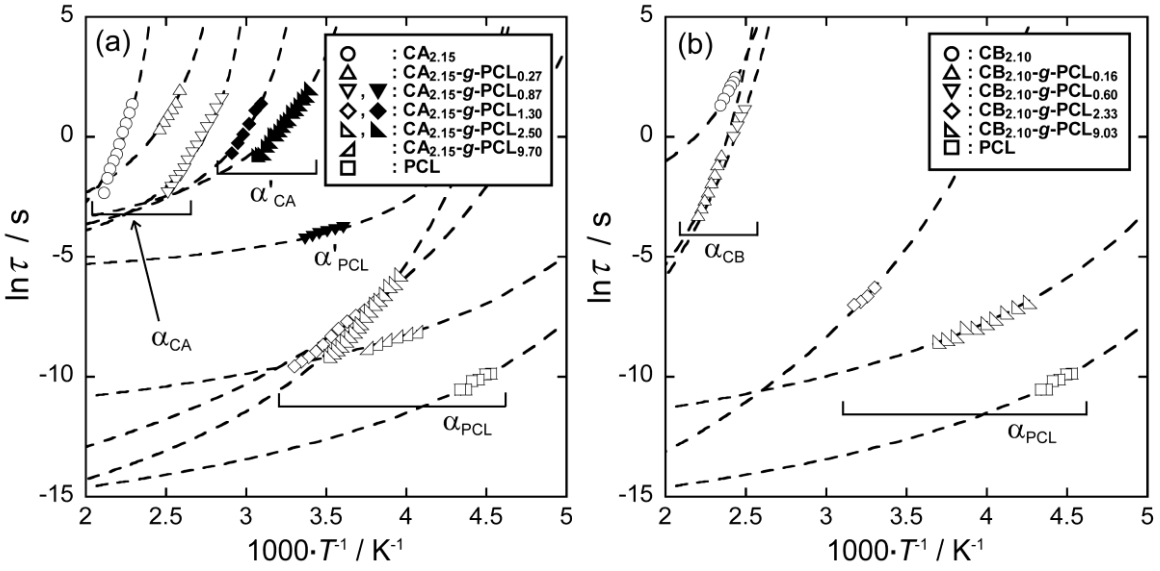

Figure 6.

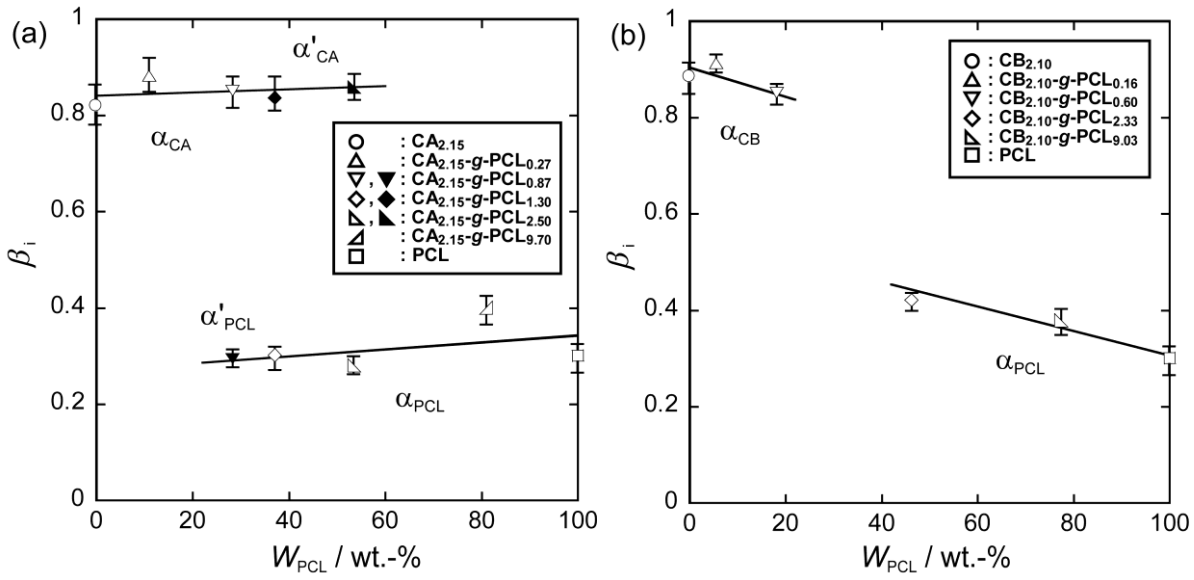

Figure 7.